Development of a Compton telescope calorimeter module for MeV-range gamma-ray astronomy

Clarisse Hamadache, Adrien Laviron, Mathieu Ehrhart, Corentin Hiver, Jürgen Kiener, Anne Meyer, Jean Peyré, Vincent Tatischeff

Development of a Compton telescope calorimeter module for MeV–range gamma–ray astronomy

Clarisse Hamadache, Adrien Laviron, Mathieu Ehrhart, Corentin Hiver, Jürgen Kiener, Anne Meyer, Jean Peyré, Vincent Tatischeff

[a] *Université Paris–Saclay, CNRS/IN2P3, IJCLab, 91405 Orsay, France,*

Abstract

Gamma-ray astronomy in the MeV energy range shows a lack of sensitivity compared to other gamma-ray energy bands. Several space observatory projects are proposed to space agencies to fill this gap. The COMCUBE CubeSat project will focus on the measurement of the polarization of the prompt emission of gamma–ray bursts (GRBs) which can provide an understanding of the physics of ultra-relativistic jets. Furthermore, the linear polarization of distant gamma–ray sources could be a probe to study the fundamental physics related to the Lorentz invariance violation. A Compton telescope is particularly well-suited for that purpose. We develop an instrument including double-sided silicon strip detectors and scintillation crystals coupled to a pixelated photodetector. The incoming photon undergoes an inelastic scattering in one or several layers of a position–sensitive silicon strip detector before being absorbed in a position–sensitive calorimeter based on inorganic scintillators. The measurement of both positions and energy deposits enables the determination of the photon's source direction. It also enables measurement of the linear polarization of the incident gamma–rays. In this contribution, we present the results of the extensive work we have carried out to develop the calorimeter and its integration into a Compton telescope prototype. We conclude by showing the first image and polarization measurements.

Keywords: gamma–ray imaging, gamma–ray polarimetry, artificial neural network, position sensitive detector, MAPMT, SiPM

1. A Compton telescope for imaging and polarimetry

The instrumental developments in gamma astronomy in the MeV energy range are a cornerstone for various scientific topics. By considering the sensitivity of gamma astronomy observatories as a function of energy, shown in figure 1, there is a lack of sensitivity around 1 MeV. In this range Compton effect is dominant, and a strong background is present. However, various scientific topics can be explored in this energy range, such as nuclear processes, compact objects, cosmic rays, and gamma–ray bursts. We can use several tools to study these phenomena, such as the temporal aspect of the emission, spectrometry, imaging, and polarimetry. The sensitivity of a future space observatory, dedicated to the MeV energy range, should be increased by one to two orders of magnitude compared to past observatories. For this purpose, we propose a novel Compton telescope composed of a silicon strip detector tracker and a position–sensitive calorimeter. The

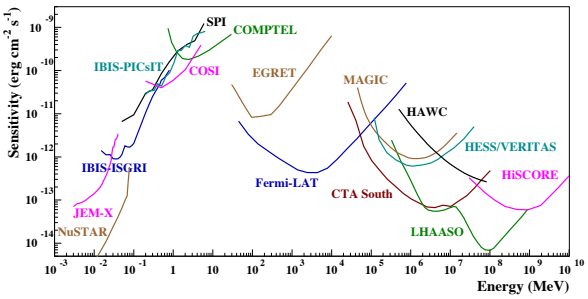

Figure 1: Sensitivity of different observatories in X - γ ray energy range (see [1])

calorimeter components are scintillators coupled with pixelated photodetectors either MultiAnodePhotomultiplier Tubes (MAPMT) or silicon PM (SiPM).

For several years we have been developing a Compton telescope which is the best concept for the science we expect. In this context, we are involved in 3 projects, currently in progress. We work in the frame-

work of an ASTROGAM–like[1] large space observatory for gamma astronomy which is a candidate for a future ESA mission. In fields other than astrophysics, we will soon achieve the ComptonCAM project. ComptonCAM is a portable gamma–camera for the nuclear industry, built on the same principle as the one for astronomy. It is dedicated to imaging the environment, planned to be used in nuclear facility removal[2]. A third project, COMCUBE, relies on a constellation of nanosatellites in low earth orbit. COMCUBE is a dedicated observatory for gamma-ray burst detection and polarimetry[3].

Instrumental requirements

A Compton telescope allows the energy and direction determination of an incoming gamma–photon by reconstructing a Compton interaction thanks to at least two layers of detectors. In our case, the first thin layer (the tracker or scatterer) favors the Compton effect and gives the position r_1 of a first energy deposit E_1. The second one, thicker (the calorimeter or the absorber), absorbs the diffused gamma–ray and gives the position r_2 of the second energy deposit E_2. We determine the incoming direction angle θ as

$$\theta = \arccos\left[1 - m_e c^2 \left(\frac{1}{E_2} - \frac{1}{E_1 + E_2}\right)\right] \quad (1)$$

where m_e is the electron mass and c the velocity of light. We then locate the origin of the incident gamma–rays as a circle in the sky from the interaction position of the gamma–rays in the detector and the energy deposits (see figure 2 left). By observing several gamma rays from one source, we localize it at the circles' intersection and image it (see figure 2 right).

A Compton telescope is also intrinsically sensitive to the linear polarization of gamma–rays. We consider the Klein–Nishina differential cross–section for linear polarization of gamma–ray

$$\frac{d\sigma_{KN}}{d\Omega} = \frac{1}{2} r_e^2 \left(\frac{E'_\gamma}{E_\gamma}\right)^2 \left[\frac{E'_\gamma}{E_\gamma} + \frac{E_\gamma}{E'_\gamma} - 2\sin^2\theta\cos^2\eta'\right] \quad (2)$$

It is a function of the electron radius r_e, the energies of the incident and diffused photons E_γ and E'_γ, and θ the diffusion angle of the diffused gamma–ray regarding the direction of the incident photon. It is also a function of η', the angle between the direction of the incoming photon's electric field and the plan of the Compton scattering. We define it as the polarisation angle η_0 with respect to a reference axis (see figure 3 top). By reconstructing the η angle, we can determine the η_0 angle as a minimum of the distribution. The source polarization fraction Π is then obtained from the modulation amplitude μ_0 compared to the ideal modulation amplitude μ_{100} for a 100% polarized gamma–ray source; the η angle distribution of an unpolarized gamma–ray source (0% polarized) being uniform (see figure 3 bottom).

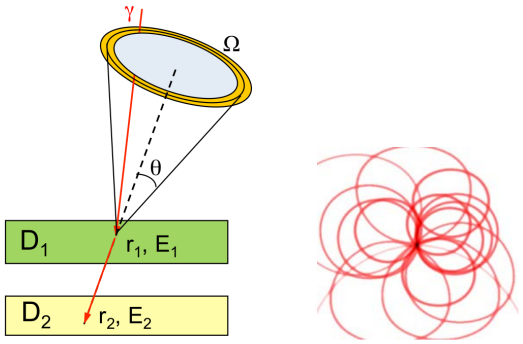

Figure 2: Compton telescope imaging principle. An incoming gamma–ray interacts by Compton effect in the first detector D_1, and the diffused photon is absorbed in the second detector D_2. The origin of the incident gamma–ray is determined as a circle in the sky from the interaction positions of the gamma–rays in the detectors and the energy deposits. Several incoming gamma–rays from the same point source give one circle's intersection that allows source imaging.

The imaging and polarimetry quality of a Compton telescope depends on the precise determination of the energy deposit and the gamma interaction localization in the tracker and the calorimeter. The tracker is made of double-sided strip detectors, so the interaction localization does not present difficulties. However, it is a primary issue in the calorimeter, which is a thick (more than 1 cm) monolithic scintillating crystal.

2. Calorimeter Module

2.1. Operation principle and machine learning tools developed for performance characterization

The type of calorimeter we study is composed of a scintillating crystal of $5 \times 5 \times 1$ to 2 cm^3, mainly cerium bromide ($CeBr_3$) crystal. It is optically coupled with a Hamamatsu photodetector, MAPMT H12700A, or SiPM array S14161–6050HS–04, both with 64 channels of 5.2×5.2 cm^2, providing a pixelated photodetector of about $6,25 \times 6,25$ mm^2 pixel size. The reading electronics is a dedicated system called ROSMAP for MAPMT and ROSSPAD for SiPM, both provided by IDEAS company (Norway). Figure 4 shows an exploded view of the module (MAPMT version).

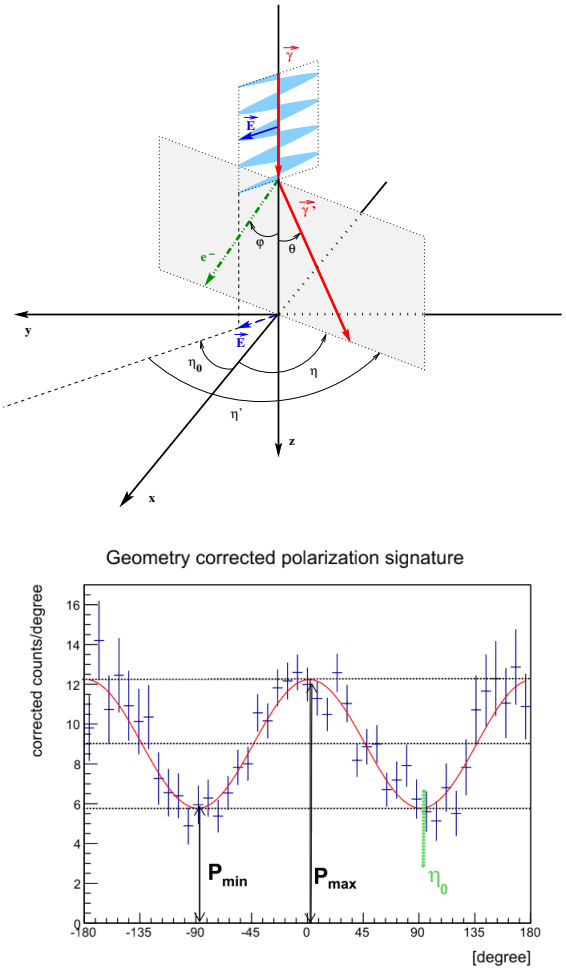

Figure 3: Polarization principle measurement. Top – Compton interaction: γ incident photon on electron e^-, and γ' diffused photon. η' is the angle between the direction of the incoming photon's electric field $\vec{E}$ and the plan of the Compton scattering. We define it as the polarisation angle η_0 with respect to a reference axis. Bottom – Polarigram: the signature of a polarization measurement. By reconstructing the η angle, we can determine the η_0 angle as a minimum of the distribution. The source polarization level Π is obtained from the amplitude $\mu_0 = (P_{max} - P_{min})/(P_{max} + P_{min})$ compared to the ideal modulation factor for a 100% polarized gamma–ray source, μ_{100}.

The principle of the position reconstruction relies on the analysis by machine learning algorithms of the scintillation light emitted. A gamma–ray penetrates the crystal and interacts at the (x,y,z) coordinates according to the defined crystal axis (figure 5, top). A part of the scintillation light emitted from the interaction point migrates toward the photodetector and is collected by its 64 pixels. We call "event" the distribution of light on the 64 pixels, represented both in 3D and 2D on the bottom of figure 5.

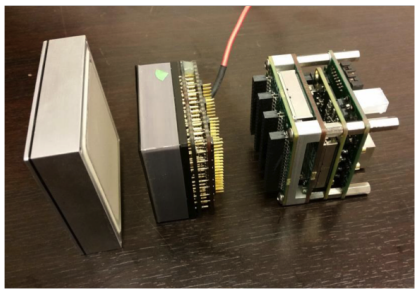

Figure 4: Picture (exploded view) of the calorimeter module. From left to right, the scintillating crystal, the MAPMT, and the read-out electronics.

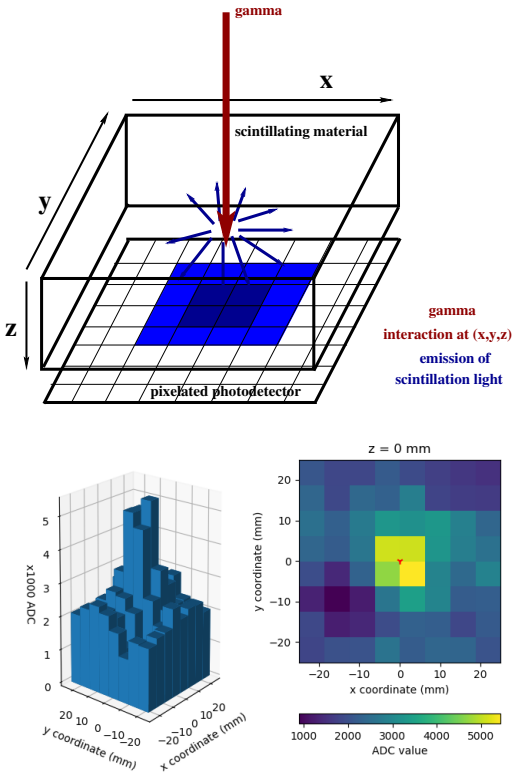

Figure 5: Top: gamma detection principle in calorimeter module; bottom: light distribution in 3D and 2D of a gamma interaction over the 64 photodetector pixels, a so–called one-peak gamma interaction localized around gamma interaction.

By analyzing the shape of the distribution light with machine learning algorithms, we reconstruct the 3D interaction position. We use a supervised learning process; the algorithms we use for localization are artificial neural networks (ANN) as multi-layer perceptrons. It means that we provide a set of events (each composed of 64 values in input corresponding to the 64 pixels) with known positions of interaction (1– z coordinates –

or 2 – (x,y) coordinates — values as output) for the first phase of training. We developed the algorithms from the Python Keras framework [4] with Theano[5] backend. After training, the resulting algorithm can reconstruct unknown positions from light distributions. The neural network architecture and parameters have been optimized by extensive data analyzing work for several gamma–ray energies and irradiation positions on the surface of the crystal (x,y position reconstruction) and also on the side of the crystal (z position reconstruction). An experimental setup called a scanning bench that provides training data is presented in figure 6; the calorimeter module is fixed on arms that move horizontally and vertically in front of a gamma–ray beam provided by a collimated radioactive source.

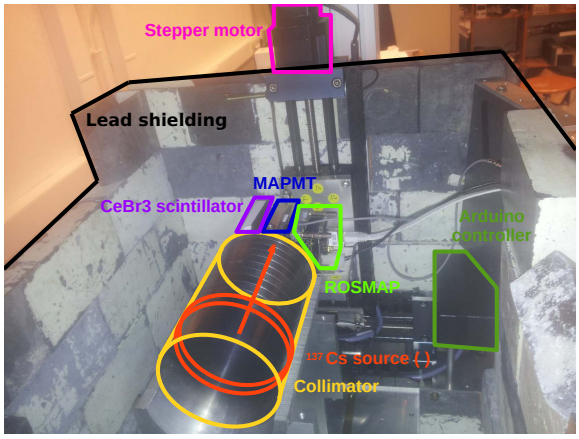

Figure 6: Scanning bench

The first stage of data analysis categorizes events into three groups:

- a so-called one-peak gamma interaction (an example is shown in the bottom of the figure 5);
- two-peaks gamma interaction (see figure 7 top);
- and the so-called scattered event (see figure 7 bottom).

The two last categories are not well reconstructed by neural network algorithms. A morphological cut based on a test of maximum pixel clusterization excludes those events; they represent less than 10% of the total number of events at 662 keV.

Once the calorimeter module was deeply studied, we obtained a spatial resolution based on the difference between the reconstruction and irradiation positions. The

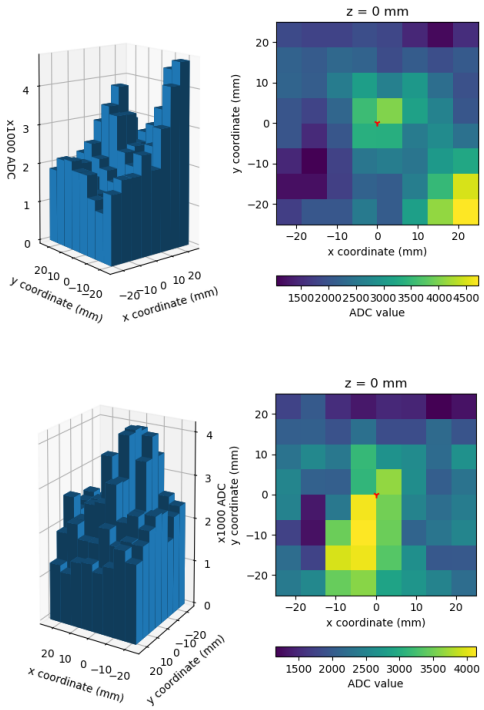

Figure 7: Two typical light distribution morphologies observed in the training data set. Top: two-peaks gamma interaction; bottom: so-called scattered event.

used root means square indicators

$$\sigma_{\mathrm{XY}} = \sqrt{\frac{1}{N_p}\sum_{i=1}^{N_p}\left[\left(x_p - x_i^{\mathrm{rec}}\right)^2 + \left(y_p - y_i^{\mathrm{rec}}\right)^2\right]}, \quad (3)$$

gives the spatial resolution calculated for the N_p event collected at the irradiation position p at coordinates (x_p, y_p) and reconstructed at the positions (x_i^{rec}, y_i^{rec}). We then determine the average 2D spatial resolution over the detection area $\overline{\sigma_{xy}} =< \sigma_{xy} >$. For z coordinates, similar indicators, σ_z and $\overline{\sigma_z}$, have been used. For a MAPMT calorimeter module, at 662 keV, the morphological selection keeps $\gtrsim$ 90 % of the events, and the spatial resolution achieves $\overline{\sigma_{xy}} \simeq 3.8$ mm, $\overline{\sigma_z} \simeq 2$ mm.

Concerning the spectrometry performance of the MAPMT calorimeter module, a raw spectrum relying on the addition of the charge collected by the 64 channels provides an energy resolution of about 8.3% at 662 keV. We then considered the dependence of the energy resolution as a function of the 2D position (x,y) of the interaction of the gamma-ray. Indeed, a larger part of the scintillation light is lost by absorption or diffusion when the gamma interaction occurs close to the crystal's

border, and therefore collected charge is lower, which leads to a degradation of the energy resolution over the 64 channels. We considered the center of the crystal as the reference position. By applying a correction factor relative to the shift in the ^{137}Cs spectral line position between the central position and the others, we obtained an energy resolution of 4.7%.

All these studies and results performed to characterize the spatial and energy resolution of the calorimeter module in the MAPMT version are published in [6].

2.2. *SiPM calorimeter module*

The MAPMTs of the calorimeter module primarily used can be replaced by a Silicon detector (SiPM). In the case of SiPM, there is no need for high voltage and, the gain of thickness reduces the volume and the mass of the instrument, which is always a significant benefit to obtain for space applications or a hand–held camera. The calorimeter module in the SiPM version is built in the same way as before; it is a cerium bromide scintillating crystal of $5 \times 5 \times 1$ cm^3 optically coupled with a Hamamatsu SiPM array of 64 pixels. The read–out electronics for SiPM is a dedicated system called ROSSPAD provided by IDEAS company (Norway). Figure 8 shows the size comparison of the two calorimeter module versions, MAPMTs vs. SiPM.

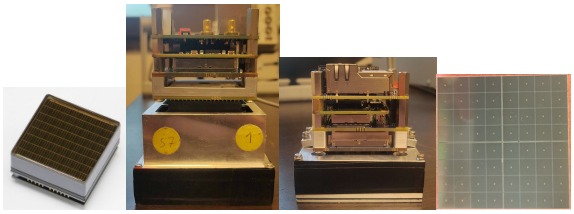

Figure 8: Complete calorimeter module version for size comparison. From left to right: picture of a MAPMT; picture of a calorimeter module, from top to bottom: electronics, MAPMT, crystal (side view); picture of a calorimeter module: the same as on the left but with a SiPM instead of a MAPMT; picture of a SiPM array.

To characterize the spectral and spatial performance of the module, we used the methods described in section 2.1. The spectral response depends on the position; there is a loss of scintillating light near the borders by absorption or diffusion. The effect is more significant at higher energy, as shown in the light map response over the SiPM surface array in figure 9.

Figure 10 shows clearly the shift in the ^{137}Cs spectral line position between the central irradiation position and two other ones closer to the borders. One can easily see the degradation in the spectral resolution by simply summing the photodetector channels. However, after

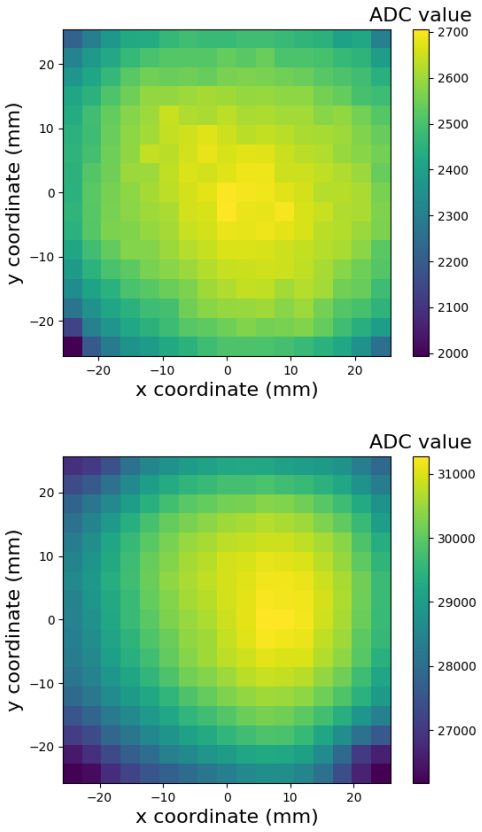

Figure 9: Relative detector spectral response through its surface measured with a collimated source and determined by the gaussian fitted energy to the spectral line for different irradiation positions spaced with a 3 mm pitch. The reference energy is the maximum of the fitted energies. Top: measurement for the 59 keV line of ^{241}Am; bottom: measurement for the 662 keV line of ^{137}Cs.

applying the correction factor as a function of the event interaction position, we obtain an energy resolution of 5% at 662 keV.

We performed the first 2D (x,y) spatial resolution study. We collected data sets for ANN training with a collimated ^{137}Cs source. We observed the three event categories shown in figure 7 in the same proportion as in section 2.1. After the reconstruction with the ANN, we plot the resulting σ_{xy} map of 2D spatial resolution at 662 keV before and after the morphological selection (see figure 11).

In figure 12, we can see the surface of the crystal (x,y coordinates); we have several irradiation positions with a gamma-ray beam, and around each irradiation position, the corresponding 3D position reconstruction of events (events are selected in energy and morphology). We observe, as expected, a degradation of the reconstruction position near the borders of the crystal.

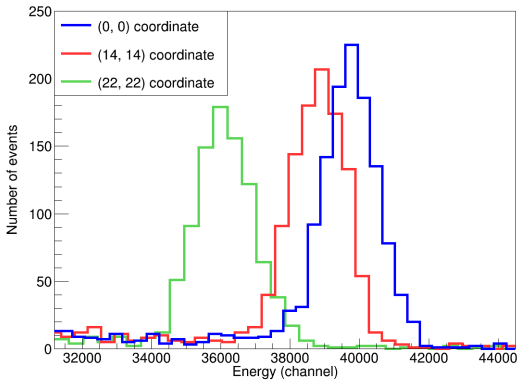

Figure 10: Spectra of the 662 keV line of a ^{137}Cs source at different irradiation positions, (0, 0) being the center of the crystal, (14, 14) an intermediary position, and (22, 22) a position close to a corner

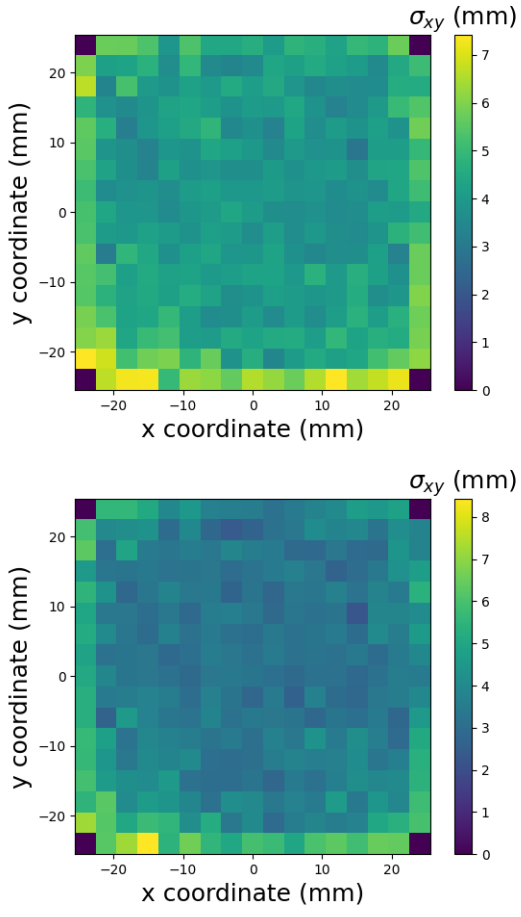

Figure 11: Spatial resolution at 662 keV, σ_{xy} map (mm) before (top) – after (bottom) morphological selection

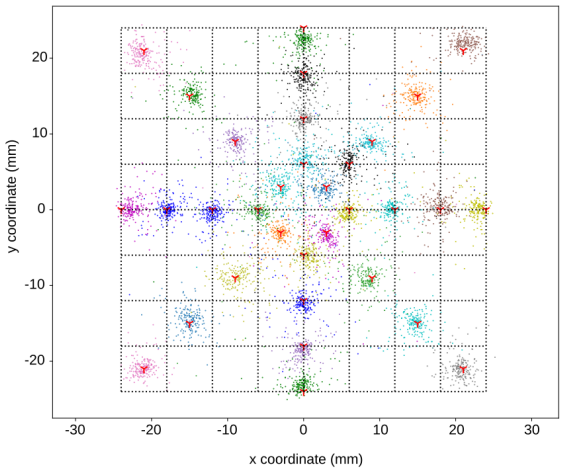

Figure 12: Example of irradiation position reconstruction by the ANN. Irradiation is made with a collimated ^{137}Cs source. Events were selected by energy (662 keV line selected) and morphology. Irradiation positions are indicated by the red markers, and gamma–rays reconstructed coordinates are shown as colored dots. A single (but not unique) color is associated with an irradiation position. Dotted black lines show the borders of the pixels.

In summary, table 1 gives the results of the 2D spatial resolution $\overline{\sigma_{xy}}$ at 662 keV for the two types of calorimeter, MAPMT version and SiPM version before and after morphological selection of the events,

	all full-E evts	morpho. selection (% rejected)
MAPMT	$\overline{\sigma_{xy}}$ = 4.20 mm	$\overline{\sigma_{xy}}$ = 3.80 mm (7%)
SiPM	$\overline{\sigma_{xy}}$ = 4.45 mm	$\overline{\sigma_{xy}}$ = 3.88 mm (7.4%)

Table 1: 2D spatial resolution $\overline{\sigma_{xy}}$ at 662 keV for both MAPMT and SiPM calorimeter versions.

The SiPM photodetector in the calorimeter module gives similar performances to those obtained with a MAPMT. It is an encouraging result for the different Compton telescopes or cameras we want to build. However, there is still work in progress to improve results and test this type of photodetector deeply to be used in astrophysical and/or high radiation environments. In the near future, we will continue working on:

- in-depth study of the electronics parameters
- spatial resolution at a larger energy range and in z–coordinate

- thermal study in a climatic chamber

2.3. *Preliminary SiPM calorimeter for space application*

For a future space observatory instrument, we need to reduce as much as possible the volume of the different components of the material. For this purpose, we are testing new electronics from Weeroc company (France) with a lower thickness than the ROSSPAD electronics described in section 2.2 (see figure 13).

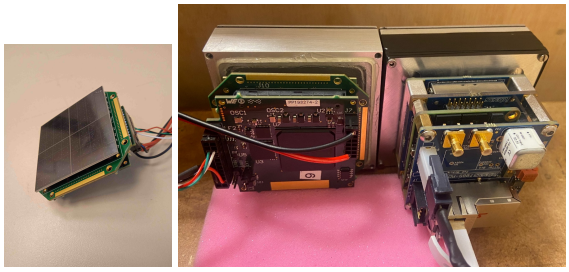

Figure 13: Left: picture of the SiPM arrays plugged with Weeroc electronics; right: picture of both SiPM calorimeter module left with the Weeroc electronics and right with the ROSSPAD electronics (for size comparison)

The Weeroc electronic module is based on the Citiroc ASICS, and several required implementations for the Compton imaging data treatment have been done (time-stamped data, regular reset time). For the COMCUBE project, the backend electronics board based on an ALTERA FPGA will be removed and replaced by a Xilinx board providing the backend electronics for all the detctors of the gamma–ray instrument. A preliminary spectrum of the collimated ^{137}Cs source is shown in figure 14; we measured an energy resolution R = 5.1%.

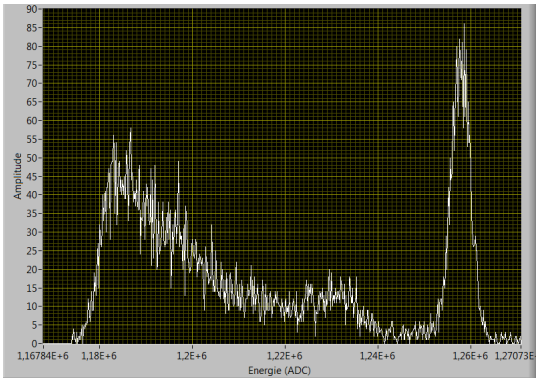

Figure 14: Preliminary spectrum with Weeroc electronics for SiPM calorimeter version. Spectral resolution is R = 5.1% at 662 keV with collimated ^{137}Cs source

3. Compton telescope prototype: first gamma image and first gamma polarization measurement

The COMCUBE collaboration is currently building a 1U CubeSat size scale model of the Compton telescope to test the performance of the proposed instrument (1U CubeSat size being $10 \times 10 \times 10$ cm^3). The main subsystems include two double–sided silicon strip detectors (DSSDs), a side calorimeter module to enhance the effective area of the telescope, a main calorimeter including four scintillating crystals, a power supply board, and a coincidence and data acquisition electronics. Important tasks for the realization of this scale model are:

- the dimensioning of the data flow and onboard storage;
- the development of the data processing software;
- the realization of the mechanical system;
- the management of the system operation and telemetry.

Before building the 1U scale model of the instrument, we did some experiments in the laboratory to test the imaging and polarimetry principle with both detector types (tracker and calorimeter) of the Compton Telescope. Figure 15 shows an image of the COMCUBE detector test bench under development. The assembly of the first DSSD with a calorimeter module allowed us to test the Compton imaging technique by making the first images of a gamma source placed at 1 m from the telescope prototype. The measured spectral resolution (6.0% FWHM at 662 keV) and angular resolution (about 7.5° FWHM at 662 keV) are in good agreement with the Compton telescope performances predicted by the numerical simulation.

A polarization measurement using a scattered gamma-ray beam is shown in Figure 16. The device, designed by numerical simulation, generates partially polarized photons of about 356 keV (theoretical polarization fraction $\Pi \simeq 60\%$). The measured polarigram (bottom) agrees with the theoretical prediction. Thus, the measurements of the signal modulation $\mu_{100}\Pi = 0.252 \pm 0.023$ and of the polarization angle $\eta_0 = 109° \pm 3°$ are consistent with the simulation results: $\mu_{100}\Pi = 0.210 \pm 0.018$ and $\eta_0 = 106° \pm 2°$. The obtained modulation factor, $\mu_{100} \simeq 0.4$, is in good agreement with the prediction for a quasi-monochromatic source of energy 356 keV observed at $\theta = 20°$. Thus, these first results of a laboratory gamma-ray polarization measurement are very promising.

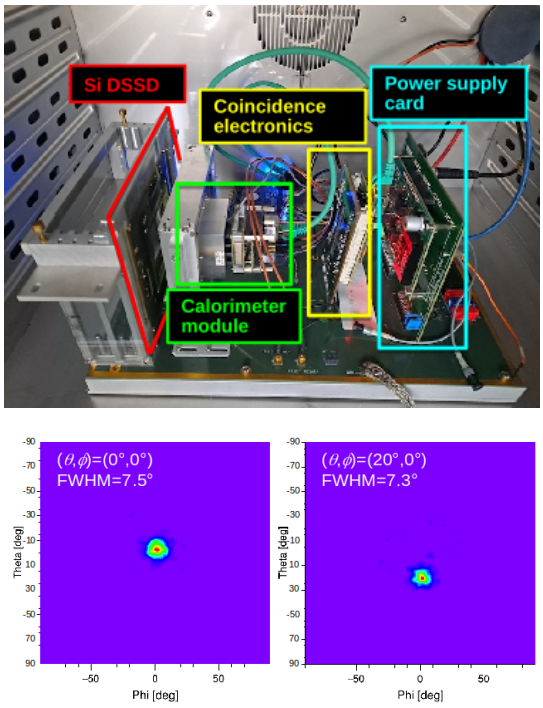

Figure 15: Top – Captioned photograph of the COMCUBE 1U prototype being assembled. The DSSD and its readout electronics are framed in red, the calorimeter module in green, the coincidence electronics in yellow and the power supply board in cyan. The telescope is placed in a climatic chamber whose temperature is regulated at 20° C. Bottom left and right - Compton images obtained with a ^{137}Cs source, (E_γ = 662keV) placed at 1 m from the telescope and at two angular positions: (θ,ϕ) = (0°,0°) (left) and (20°,0°) (right).

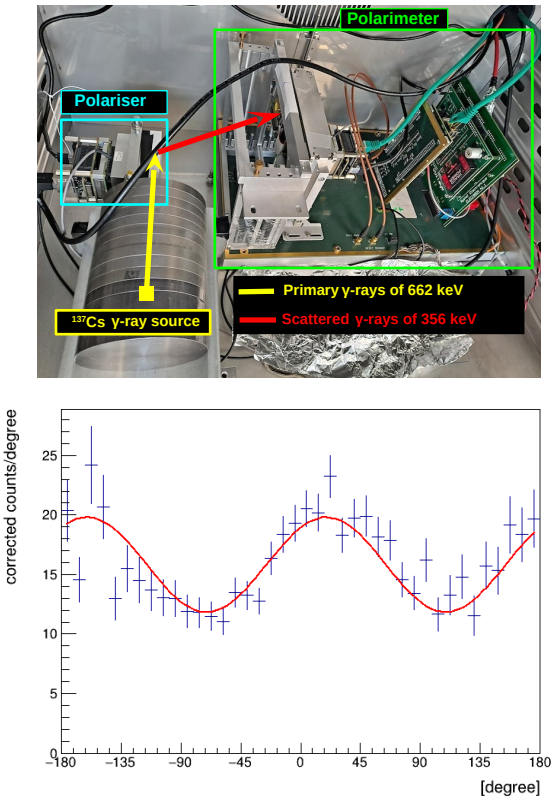

Figure 16: Top: captioned picture of the experimental setup used to test the COMCUBE 1U prototype at the polarization measurement. Bottom: polarigram, i.e., distribution of azimuthal Compton scattering angles corrected for systematic effects due to the asymmetric response function of the polarimeter.

4. Conclusion and future works

After testing the 1U model in the laboratory, the collaboration wishes to carry out an onboard stratospheric balloon experiment to gain operational experience with the instrument in the near-space environment. In particular, we wish to test the detection of an astrophysical source - the Crab nebula and pulsar - in a background of radiation and cosmic particles representative of that in low Earth orbit. We will also study the radiation hardness of the detectors and other payload components and their operation in an environment with a temperature range similar to that found in low earth orbit.

Acknowledgments

This work is supported by the European Union's Horizon 2020 Program under the AHEAD2020 project (grant agreement n. 871158), and by Andra under the "Investing in the Future Program" of the French Government.

References

[1] A. De Angelis, V. Tatischeff, et al., The e-ASTROGAM mission. Exploring the extreme Universe with gamma rays in the MeV - GeV range, Experimental Astronomy 44 (1) (2017) 25–82. arXiv:1611.02232, doi:10.1007/s10686-017-9533-6.

[2] V. Tatischeff, et al., ComptonCAM, `https://international.andra.fr/sites/international/files/2019-08/Fiche%20projet%20COMPTON-CAM%20UK.pdf` (2019).

[3] A. Laviron, et al., COMCUBE: A constellation of CubeSats to measure the GRB prompt emission polarization, in: SF2A-2021: Proceedings of the Annual meeting of the French Society of Astronomy and Astrophysics. Eds.: A. Siebert, 2021, pp. 105–108.

[4] F. Chollet, et al., Keras, `https://keras.io` (2015).

[5] The Theano Development Team, et al., Theano: A Python framework for fast computation of mathematical expressions, arXiv e-prints (2016) arXiv:1605.02688arXiv:1605.02688.

[6] A. Laviron, V. Gourlaouen, C. Hamadache, C. Hiver, J. Kiener, J. Peyré, V. Tatischeff, Optimization of $CeBr_3$ position-sensitive calorimeter module, Nuclear Instruments and Methods in Physics Research A 1007 (2021) 165379. doi:10.1016/j.nima.2021.165379.